Polymer 50 (2009) 1805–1813

Contents lists available at ScienceDirect

Polymer

journal homepage: www.elsevier.com/locate/polymer

Effect of the counterion behavior on the frictional–compressive properties of chondroitin sulfate solutions

S.A. Baeurle [a,*], M.G. Kiselev [b], E.S. Makarova [b], E.A. Nogovitsin [b]

[a] Department of Chemistry and Pharmacy, Institute of Physical and Theoretical Chemistry, University of Regensburg, Universitaetsstrasse 31, D-93053 Regensburg, Germany
[b] Institute of Solution Chemistry, Russian Academy of Sciences, 153045 Ivanovo, Russia

ARTICLE INFO

Article history:
Received 20 October 2008
Received in revised form
28 January 2009
Accepted 30 January 2009
Available online 10 February 2009

Keywords:
Field-theoretic calculation
Chondroitin sulfate solutions
Counterion behavior

ABSTRACT

Chondroitin sulfate is a major constituent of articular cartilage, which is known to affect in a decisive way the mobility and flexibility of our joints. A deviation from the physiological conditions, like e.g. a deficiency of water and salt content, in the cartilage tissue has long been suspected to be a possible trigger for rheumatoid diseases. Progresses in understanding the frictional–compressive behavior on the molecular level have been hindered due to the lack of reliable experimental data and the multitude of controlling parameters, influencing the structure and properties of cartilage tissue in its natural environment. In this paper we study the thermodynamic response of aqueous chondroitin sulfate solutions to changes in the monomer and added salt concentrations, using a recently developed field-theoretic approach beyond the mean field (MF) level of approximation. Our approach relies on the method of Gaussian equivalent representation, which has recently been shown to provide reliable thermodynamic information for polyelectrolyte solutions without and with added salt over the whole range of monomer concentrations. We compare our calculation results to experimental as well as molecular modeling data, and demonstrate that it provides useful estimates for important thermodynamic properties. Moreover, we obtain conclusive insights about the hydration effects and counterion behavior under various conditions, which show that, at the physiological salt concentration, CS solutions have optimal compressive and tribological properties. Finally, our work provides support for the possibility that a long-term deviation from the physiological conditions may trigger rheumatoid diseases.

1. Introduction

Articular cartilage is a hydrated soft tissue composed of negatively charged proteoglycans fixed within a collagen matrix, whose primary function is to provide low friction and wear in the synovial joints. A charge gradient causes the tissue to absorb water and swell, creating a net osmotic pressure that is counteracted by the resistance of the network of collagen fibers [1]. This confers cartilage its characteristic mechanical properties of being able to resist high loads and tensile strains. Joint loading is known to be a combination of cartilage compression and shear, including all transversal and frictional forces [2]. It is primarily controlled by large proteoglycan molecules called aggrecans, which interact with a long hyaluronic acid carbohydrate to form aggregates of very high molecular weight. A single aggrecan molecule is composed of a protein backbone of 210–250 kDa, to which are attached long negatively charged polysaccharide molecules, so-called glycosaminoglycans (GAGs), with a molecular weight ranging from 10 to 40 kDa. A schematic representation of an aggrecan monomer and its aggregate is shown in Fig. 1. The predominant type of GAG in aggrecan is *chondroitin sulfate* (CS). It is a linear polysaccharide with alternating disaccharide units of glucuronic acid and N-acetylgalactosamine [3], whose chemical composition can vary, depending on the state of health or disease of the cartilage tissue [1,4,5]. The physiologically important CS's are in particular chondroitin 4-sulfate (C4S) and chondroitin 6-sulfate (C6S), for which the sulfate group is either located at the C4- or C6-position of the galactosamine residue, respectively.

Systems composed of CS have been the subject of various experimental as well as theoretical investigations, both in solution [1,3,5,6,7] as well as in cartilage [3]. Extensive thermodynamic investigations on aqueous CS solutions have recently been presented by Chahine et al. [1], who performed direct experimental measurements of the osmotic pressure using membrane osmometry. Their experiments were conducted with solutions of CS-C (89.6% C6S and 10.3% C4S) and CS-A (39% C6S and 61% C4S).

* Corresponding author. Tel.: +49 941 943 4470.
E-mail address: stephan.baeurle@chemie.uni-regensburg.de (S.A. Baeurle).

0032-3861/$ – see front matter © 2009 Elsevier Ltd. All rights reserved.
doi:10.1016/j.polymer.2009.01.066

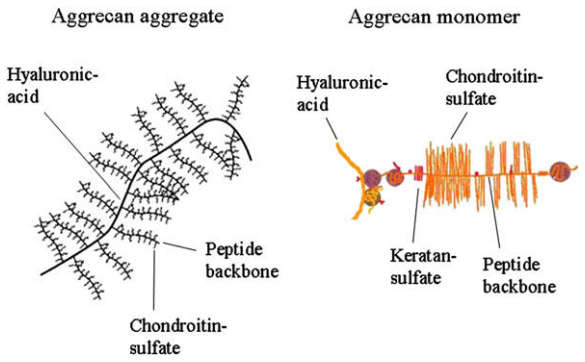

Fig. 1. Aggrecan monomer and its aggregate.

They concluded from their study that the osmotic pressure grows nonlinearly with increasing CS concentration and decreasing ionic strength of the NaCl bath. Moreover, they found that the differences in the osmotic pressure of the CS-C and CS-A solutions are negligible. From the theoretical side, Bathe et al. [5] carried out molecular modeling investigations using a Metropolis Monte Carlo algorithm, to determine the osmotic pressure of C4S and C6S solutions at various monomer concentrations and reservoir ionic strengths. To represent their data, Bathe et al. used a virial expansion, which allowed them to quantify the extent of nonideality in the dilute and semidilute regimes for different chain lengths. They compared their predictions to the experimental results of Ehrlich et al. [8] and various theoretical models, including the Donnan theory [9] and the Poisson–Boltzmann cylindrical cell model [10]. A major conclusion from their work is that their modeling predictions only agree qualitatively with the experimental results of Ehrlich et al. and Chahine et al., as well as with the results from the theoretical models mentioned previously. Another important outcome is that the steric excluded volume plays a negligible role in the CS osmotic pressure at the physiological ionic strength. This relates to the dominance of the repulsive electrostatic interactions that maintain the chains in this regime maximally spaced, whereas at high-ionic strengths the steric interactions dominate due to electrostatic screening. Finally, they found, in agreement with the experimental measurements of Chahine et al. on CS-C and CS-A solutions, that the position of the sulfate group in C4S and C6S solutions has only a minor effect on the osmotic pressure. In a concerted experimental and theoretical investigation of the mechanical behavior of cartilage Jin and Grodzinsky discovered that the electrostatic interactions between the GAG molecules have a major influence on the shear properties of the cartilage tissue in the extracellular matrix [11]. In a recent work Basalo et al. [3] found that CS decreases the friction coefficient of articular cartilage by performing frictional tests and concluded that the underlying mechanism is neither mediated by viscosity nor osmotic pressure. Based on these findings, they suggested that a direct injection of CS into the joints may be beneficial for their tribological properties.

In the present study our goal is to understand the role and assess the influence of CS on the frictional–compressive properties of articular cartilage. To this end, we investigate the response of the thermodynamic properties of aqueous CS solutions to changes in the monomer as well as salt concentrations. We put a particular focus on the central issue of counterion condensation onto the CS chains, which we suspect to be responsible for the reduction of the friction coefficient in articular cartilage [3]. The counterion condensation phenomenon is commonly described by Manning's theory [12], which assumes that counterions can *condense* onto the polyions until the charged density between neighboring monomer charges along the polyion chain is reduced below a certain critical value. In the model the real polyion chain is replaced by an idealized line charge, where the polyion is represented by a uniformly charged thread of zero radius, infinite length and finite charge density, and the condensed counterion layer is assumed to be in physical equilibrium with the ionic atmosphere surrounding the polyion. The uncondensed mobile ions in the ionic atmosphere are treated within the Debye–Hückel (DH) approximation. The phenomenon of counterion condensation now takes place when the dimensionless Coulomb coupling strength $\Gamma = \lambda_B/l_{charge} > 1$, where λ_B represents the Bjerrum length and l_{charge} the distance between neighboring charged monomers [13]. In this case the Coulomb interactions dominate over the thermal interactions and counterion condensation is favored. For many standard polyelectrolytes, this phenomenon is relevant, since the distance between neighboring monomer charges typically ranges between 2 and 3 Å and $\lambda_B \approx 7$ Å in water. In the case of CS systems $\Gamma = 1.4$, which implies that counterion condensation should take place. However, Bathe et al. [7] have recently performed simulations with fully ionized CS chains. They validated their approach by noting that CS systems are a borderline case and Manning's theory does not take into account the molecular details of real polyion chains, like e.g. local solvation effects or atomic partial charge distributions.

In the present paper our goal is to investigate the counterion condensation phenomenon in CS solutions at different monomer and salt concentrations and study the influence of solvation effects on the frictional–compressive properties of CS polyelectrolytes in solution and cartilage. Our investigations are carried out, using the field-theoretic approach for flexible polyelectrolyte chains introduced by us in Ref. [14]. In the latter work we employed the tadpole renormalization procedure making use of the method of Gaussian equivalent representation (GER) for functional integrals [14,15,16], which goes beyond the MF level of approximation. In particular, we demonstrated that the GER methodology provides useful osmotic pressure results for polyelectrolyte solutions composed of sodium poly(styrene-sulfonate) (NaPSS) without and with added salt over the whole range of monomer concentrations.

Our paper is organized in the following way. In Section 2 we review the basic derivation of the field theory for flexible polymer chains, followed by the derivation of our GER theory. Then, we demonstrate the applicability of the method on systems of polyelectrolyte chains, where the monomers interact via the electrostatic part of the Derjaguin–Landau–Verwey–Overbeek (DLVO) pair potential [17,18], and develop the corresponding formulas, employed to calculate the structural and thermodynamic quantities considered in this work. In Section 3 we present and discuss the results of our calculations on the example of aqueous C4S solutions at various monomer and salt concentrations by comparing them to the osmotic pressure measurements of Chahine et al. [1] and the molecular modeling data of Bathe et al. [5].

2. Theory

2.1. Field theory for flexible polymer chains

In this work we treat the aqueous polyelectrolyte solutions within the standard continuum model of Edwards for flexible polymer chains, dissolved in a good solvent [19]. The macromolecules are assumed to be linear homopolymers of uniform length with statistical properties, described by the continuous Gaussian chain model. The solvent degrees of freedom are not

explicitly taken into account in the statistical mechanical description, but will be introduced *a posteriori* in a coarse-grained fashion. The interactions among the segments are assumed to be characterized by the electrostatic part of the DLVO potential. For this model, the grand canonical partition function at temperature T and volume V can be formulated as follows:

$$\Xi(z,V,T) = \sum_{n=0}^{\infty}\frac{z^n}{n!}\int\delta\mathbf{r}_1\ldots\int\delta\mathbf{r}_n\exp\left[-\beta\Phi_0[\mathbf{r}]-\beta\Phi_1[\mathbf{r}]\right], \tag{1}$$

with $\beta = 1/(k_BT)$ and n representing the number of polymers. The activity

$$z = \frac{1}{\lambda_T^3}e^{\beta\mu}, \tag{2}$$

where μ is the chemical potential and $\lambda_T = h(\beta/(2\pi m))^{1/2}$ is the thermal de-Broglie wavelength with m as the mass of the polymers. The notation $\int\delta\mathbf{r}_1\ldots\int\delta\mathbf{r}_n$ denotes n path integrals over all possible space curves, where the polymer coordinates $\mathbf{r}_i\in R^3$ with $i=1,\ldots,n$ describe the conformations of the chains. The energy contributions, representing the short-ranged harmonic binding interactions, are contained in the following term

$$\Phi_0[\mathbf{r}] = \frac{3}{2\beta Nb^2}\sum_{l=0}^{n}\int_0^1 ds\left|\frac{d\mathbf{r}_l(s)}{ds}\right|^2, \tag{3}$$

where N is the polymerization index and b is the statistical segment length. The potential energy contribution

$$\Phi_1[\mathbf{r}] = \frac{1}{2}\int d\mathbf{r}\int d\mathbf{r}'\widehat{\rho}(\mathbf{r})\Phi_1(|\mathbf{r}-\mathbf{r}'|)\widehat{\rho}(\mathbf{r}') - \frac{1}{2}nN\Phi_1(0) \tag{4}$$

describes the long-range interactions between the monomers, where

$$\widehat{\rho}(\mathbf{r}) = N\sum_{j=1}^{n}\int_0^1 ds\,\delta\left(\mathbf{r}-\mathbf{r}_j(s)\right) \tag{5}$$

represents the segment density operator. To introduce the auxiliary field w, let us in the following make use of a functional form of the Hubbard–Stratonovich transformation [20]

$$e^{-\frac{\beta}{2}\left(\widehat{\rho}\Phi_1\widehat{\rho}\right)} = \int\frac{\delta w}{\sqrt{\det\Phi_1}}e^{-\frac{1}{2}\left(w\Phi_1^{-1}w\right)+i\sqrt{\beta}\left(\widehat{\rho}w\right)}, \tag{6}$$

where

$$e^{-\frac{\beta}{2}\left(\widehat{\rho}\Phi_1\widehat{\rho}\right)} = \exp\left[-\frac{\beta}{2}\int d\mathbf{r}\int d\mathbf{r}'\widehat{\rho}(\mathbf{r})\Phi_1(\mathbf{r}-\mathbf{r}')\widehat{\rho}(\mathbf{r}')\right],$$

$$\left(w\Phi_1^{-1}w\right) = \frac{1}{V^2}\int d\mathbf{r}\int d\mathbf{r}'w(\mathbf{r})\Phi_1^{-1}(\mathbf{r}-\mathbf{r}')w(\mathbf{r}'),$$

$$\left(\widehat{\rho}w\right) = \int d\mathbf{r}\widehat{\rho}(\mathbf{r})w(\mathbf{r}) = N\sum_{j=0}^{n}\int_0^1 ds\,w\left(\mathbf{r}_j(s)\right). \tag{7}$$

This provides us the grand canonical partition function in its basic field-theoretic representation [14]

$$\Xi(z,V,T) = \int\frac{\delta w}{\sqrt{\det\Phi_1}}e^{-\frac{1}{2}\left(w\Phi_1^{-1}w\right)+\tilde{z}VQ[iw]}, \tag{8}$$

where

$$Q[iw] = \frac{\int\delta\mathbf{r}\exp\left[-\frac{3}{2Nb^2}\int_0^1 ds\left|\frac{d\mathbf{r}(s)}{ds}\right|^2+iN\sqrt{\beta}\int_0^1 ds\,w(\mathbf{r}(s))\right]}{\int\delta\mathbf{r}\exp\left[-\frac{3}{2Nb^2}\int_0^1 ds\left|\frac{d\mathbf{r}(s)}{ds}\right|^2\right]} \tag{9}$$

is the partition function of a single polymer with

$$\tilde{z} = \frac{\exp[\beta\mu+\frac{\beta}{2}N\Phi_1(0)]}{\lambda_T^{3N}}\int\delta\mathbf{r}\exp\left[-\frac{3}{2Nb^2}\int_0^1 ds\left|\frac{d\mathbf{r}(s)}{ds}\right|^2\right] \tag{10}$$

as the polymer activity. Note that for $V\to\infty$ we have

$$\frac{1}{\sqrt{\det\Phi_1}} = \exp\left[-\frac{V}{2}\int\frac{d\mathbf{p}}{(2\pi)^3}\ln\Phi_1(\mathbf{p})\right], \tag{11}$$

with

$$\Phi_1(\mathbf{p}) = \tilde{\Phi}_1(\mathbf{p})/V$$

and

$$\tilde{\Phi}_1(\mathbf{p}) = \int d\mathbf{r}\,\Phi_1(\mathbf{r})e^{i(\mathbf{pr})}, \tag{12}$$

$$\Phi_1(\mathbf{r}) = \int\frac{d\mathbf{p}}{(2\pi)^3}\tilde{\Phi}_1(\mathbf{p})e^{-i(\mathbf{pr})}.$$

2.2. Gaussian equivalent representation and its 0th-order approximation

To derive the GER of the grand canonical partition function, let us perform the following shift of the integration contour

$$w(\mathbf{r})\to w(\mathbf{r})+\frac{i}{\sqrt{\beta}}c_{GER}, \tag{13}$$

where c_{GER} represents the shifting function, and transform the Gaussian measure in the following way [16]

$$d\mu_{\Phi_1} = \int\frac{\delta w}{\sqrt{\det\Phi_1}}e^{-\frac{1}{2}\left(w\Phi_1^{-1}w\right)}\to d\mu_D = \int\frac{\delta w}{\sqrt{\det D}}e^{-\frac{1}{2}\left(wD^{-1}w\right)}, \tag{14}$$

where $D(\mathbf{r}-\mathbf{r}')$ is a renormalized effective interaction potential. Our basic idea is to remove the divergent self-interaction contributions from the interaction functional in Eq. (8). We achieve this by applying the concept of normal product [16] and requiring that the linear and quadratic normal products of the field variable $w(\mathbf{r})$ are absent in the new integrant exponent. As a result, we obtain the GER of the grand canonical partition function [21]

$$\Xi(z,V,\beta) = e^{-\beta\Omega_{GER}^0}\int d\mu_D[w]e^{W[w]}, \tag{15}$$

where

$$W[w] = \frac{c_{GER}}{\beta\tilde{\Phi}(\mathbf{p}=0)}\int d\mathbf{r}\left[e^{i\sqrt{\beta}w(\mathbf{r})+\frac{\beta}{2}D(0)}-1-i\sqrt{\beta}w(\mathbf{r})+\frac{\beta}{2}\left(w^2(\mathbf{r})-D(0)\right)\right]. \tag{16}$$

The shifting parameter c_{GER} and renormalized potential $D(\mathbf{r}-\mathbf{r}')$ are obtained by solving the so-called GER equations [16,21,22]

$$c_{\mathrm{GER}} = \frac{z_1 N\beta\tilde{\Phi}_1(\mathbf{p}=0)}{V}\mathrm{e}^{-Nc_{\mathrm{GER}}}, \tag{17}$$

$$\tilde{D}(\mathbf{p}) = \frac{\tilde{\Phi}_1(\mathbf{p})}{1+Nc_{\mathrm{GER}}\left(\frac{\tilde{\Phi}_1(\mathbf{p})}{\tilde{\Phi}_1(\mathbf{p}=0)}\right)},$$

where

$$z_1 = \frac{\exp[\beta\mu+\frac{\beta}{2}N(\Phi_1(0)-D(0))]}{\lambda_T^{3N}}\int\delta\mathbf{r}\,\exp\left[-\frac{3}{2Nb^2}\int_0^1 \mathrm{d}s\left|\frac{\mathrm{d}\mathbf{r}(s)}{\mathrm{d}s}\right|^2\right] \tag{18}$$

and

$$D(\mathbf{r}-\mathbf{r}') = \int\frac{\mathrm{d}\mathbf{p}}{(2\pi)^3}\tilde{D}(\mathbf{p})\mathrm{e}^{-i\mathbf{p}(\mathbf{r}-\mathbf{r}')} \tag{19}$$

represents the potential of mean-force within the GER formalism [15]. Moreover, the function Ω^0_{GER} defines the grand canonical free energy in the 0th-order GER (GER0) approximation and is given by

$$\Omega^0_{\mathrm{GER}} = -\frac{V}{2\beta}\int\frac{\mathrm{d}\mathbf{p}}{(2\pi)^3}\left[\ln\left(\frac{\tilde{D}(\mathbf{p})}{\tilde{\Phi}_1(\mathbf{p})}\right)-\frac{\tilde{D}(\mathbf{p})}{\tilde{\Phi}_1(\mathbf{p})}+1\right] - \frac{V(2c_{\mathrm{GER}}+c^2_{\mathrm{GER}})}{2\beta^2\tilde{\Phi}_1(\mathbf{p}=0)}. \tag{20}$$

2.3. Monomer interaction model

In the following we assume that the effective interactions between the monomers can suitably be described by the electrostatic part of the DLVO-pair potential given by

$$\Phi_1(r) = \frac{z^2_{\mathrm{M}}A(\kappa,a)\lambda_{\mathrm{B}}}{\beta}\frac{\mathrm{e}^{-\kappa r}}{r}, \tag{21}$$

where $r=|\mathbf{r}|$ is the distance between the monomer centers and $\lambda_{\mathrm{B}}=e^2/(\epsilon k_{\mathrm{B}}T)$ is the Bjerrum length with e and ϵ as the elementary charge and dielectric constant of the suspending medium, respectively. Moreover, z_{M} is the monomer charge number and

$$A(\kappa,a) = \left(\frac{\exp(\kappa a/2)}{1+\kappa a/2}\right)^2 \tag{22}$$

is the geometrical factor, where a denotes the diameter of the sphere encompassing the *excluded volume* of a monomer. The screening parameter κ governs the range of interactions and is given by $\kappa=\sqrt{8\pi\lambda_{\mathrm{B}}I}$ with the ionic strength

$$I = \frac{1}{2}\left[\sum_c z_c^2\langle\rho_c\rangle+\sum_i z_i^2\langle\rho_i\rangle\right], \tag{23}$$

where $\langle\rho_c\rangle$ is the density of the counterions with charge number z_c and $\langle\rho_i\rangle$ is the density of the added salt ions with charge number z_i. The Fourier transform of the DLVO potential is

$$\tilde{\Phi}_1(p) = \frac{4\pi z^2_{\mathrm{M}}A(\kappa,a)\lambda_{\mathrm{B}}}{\beta}\frac{1}{p^2+\kappa^2}, \tag{24}$$

with the length of the reciprocal lattice vector $p=|\mathbf{p}|$.

2.4. Thermodynamic and structural quantities

As demonstrated in Ref. [23], thermodynamic properties within the GER0 formalism can easily be derived via the free energy route (F-route) or the pair distribution function route (g-route). Within the F-route, the GER0 approximation of the osmotic pressure takes the form

$$\Pi = -\frac{\Omega}{V} = \frac{1}{(2\pi)^2\beta}\int_0^\infty \mathrm{d}p p^2\left[\frac{\tilde{c}_{\mathrm{GER}}\upsilon(p)}{1+\tilde{c}_{\mathrm{GER}}\upsilon(p)}-\ln\left(1+\tilde{c}_{\mathrm{GER}}\upsilon(p)\right)\right] + \frac{\tilde{c}^2_{\mathrm{GER}}+2\tilde{c}_{\mathrm{GER}}}{2\beta^2N^2\tilde{\Phi}_1(p=0)}, \tag{25}$$

where the GER0 approximation of Ω is given by Eq. (20) with $\upsilon(p)=\tilde{\Phi}_1(p)/\tilde{\Phi}_1(p=0)$ and $\tilde{c}_{\mathrm{GER}}=Nc_{\mathrm{GER}}$. The average polymer density is derived via the following formula:

$$\langle\rho\rangle = \frac{z_1}{V}\frac{1}{\Xi}\left(\frac{\partial\Xi}{\partial z_1}\right)_{\beta,V} = \frac{\beta\tilde{c}_{\mathrm{GER}}}{1+\tilde{c}_{\mathrm{GER}}}\left(\frac{\partial\Pi}{\partial\tilde{c}_{\mathrm{GER}}}\right)_{\beta,V}. \tag{26}$$

Inserting the DLVO potential Eq. (21) into the Eqs. (17) written in terms of $\tilde{c}_{\mathrm{GER}}$ and Eq. (26), we can express the average polymer density as

$$\langle\rho\rangle = \frac{\tilde{c}_{\mathrm{GER}}N_{\mathrm{A}}}{N^2B}-\frac{\kappa^3\tilde{c}^2_{\mathrm{GER}}}{16\pi\left(1+\tilde{c}_{\mathrm{GER}}\right)^{3/2}}, \tag{27}$$

where

$$B = 4\pi z^2_{\mathrm{M}}A(\kappa,a)\lambda_{\mathrm{B}}N_{\mathrm{A}}/\kappa^2 \tag{28}$$

and N_{A} is the Avogadro constant. The monomolar concentration is defined via $C_{\mathrm{M}}=N\langle\rho\rangle/N_{\mathrm{A}}$ and yields

$$C_{\mathrm{M}} = \frac{\tilde{c}_{\mathrm{GER}}}{NB}-\frac{N\kappa^3}{16\pi N_{\mathrm{A}}}\frac{\tilde{c}^2_{\mathrm{GER}}}{\left(1+\tilde{c}_{\mathrm{GER}}\right)^{3/2}}. \tag{29}$$

Note that the previous equation defines the contour shift parameter $\tilde{c}_{\mathrm{GER}}$ as a function of monomer concentration and the polymerization index N. Using it to reformulate the osmotic pressure in Eq. (25), we get

$$\frac{\Pi}{RT} = \frac{C_{\mathrm{M}}}{N}+\frac{C^2_{\mathrm{M}}}{N^2}\eta(\kappa,a), \tag{30}$$

where R is the molar ideal gas constant, while

$$\eta(\kappa,a) = \frac{2}{3}\pi z^2_{\mathrm{M}}A(\kappa,a)N_{\mathrm{A}}\lambda_{\mathrm{B}}\int_0^\infty \mathrm{d}r\, rg(r)(1+\kappa r)\mathrm{e}^{-\kappa r}, \tag{31}$$

with the GER0 approximation of the radial distribution function [21]

$$g(r) = \mathrm{e}^{-\beta D(r)} \tag{32}$$

and

$$D(r) = \frac{4\pi z^2_{\mathrm{M}}A(\kappa,a)\lambda_{\mathrm{B}}}{\beta}\frac{\mathrm{e}^{-\kappa r\sqrt{1+\tilde{c}_{\mathrm{GER}}}}}{r}. \tag{33}$$

The entropy can be formulated as [24]

$$s = s^{\mathrm{id}} + \frac{1}{2}k_{\mathrm{B}}\beta n \int \mathrm{d}\mathbf{r}\, \Phi_1(r)\left[g(r) - 1 - \int_0^1 \mathrm{d}\lambda \nu_2(r,\lambda)\right], \qquad (34)$$

where s^{id} is the entropy of the ideal gas and $g(r)$ is given by Eq. (32), while $\nu_2(r,\lambda) = g(r,\lambda) - 1 = \mathrm{e}^{-\beta D(r,\lambda)} - 1$ with

$$D(r,\lambda) = \frac{4\pi z_{\mathrm{M}}^2 A(\kappa,a)\lambda_{\mathrm{B}}\lambda}{\beta}\frac{\mathrm{e}^{-\kappa r\sqrt{1+\bar{c}_{\mathrm{GER}}}}}{r}. \qquad (35)$$

Using the GER0 approximation of the monomer concentration in Eq. (29) and the entropy expression in Eq. (34), we obtain the molar excess entropy as

$$s_{\mathrm{m}}^{\mathrm{ex}} = \frac{1}{2}k_{\mathrm{B}}\beta C_M \int \mathrm{d}\mathbf{r}\, \Phi_1(r)\left[g(r) - 1 - \int_0^1 \mathrm{d}\lambda\, \nu_2(r,\lambda)\right]. \qquad (36)$$

3. Results and discussion

In the following we present GER0 calculations for aqueous CS solutions at different NaCl concentrations and compare the results to the osmotic pressure measurements of Chahine et al. [1], as well as the molecular modeling data of Bathe et al. [5]. For comparison, we considered only C4S solutions, because the differences in the osmotic pressure of the C4S and C6S solutions, as well as of their mixtures, were found to be negligible. Note that we did not take into account the osmotic pressure results of Ehrlich et al. in our theoretical analysis [8], because they performed their experiments at a temperature of 277 K, in contrast to room temperature in case of Chahine et al. Moreover, their results have been found to be sensitive to their indirect technique of measurement [1], which consists in equilibrating CS solutions placed in dialysis sacs against polyethylene glycol (PEG) solutions of known concentrations and deducing the osmotic pressures of the CS solutions from the calibrated PEG osmotic pressures. In our calculations we invoked electroneutrality, which implies that

$$z_{\mathrm{H}}C_{\mathrm{H}} + z_{\mathrm{M}}C_{\mathrm{M}} + z_{\mathrm{Na}}C_{\mathrm{Na}} + z_{\mathrm{Cl}}C_{\mathrm{Cl}} = 0, \qquad (37)$$

where the charges and concentrations for the H^+-, Na^+-, Cl^--ions and the CS disaccharide repeat (monomeric) units are, respectively, given by $z_{\mathrm{H}} = +1$, C_{H}, $z_{\mathrm{Na}} = +1$, C_{Na}, $z_{\mathrm{Cl}} = -1$, C_{Cl}, $z_{\mathrm{M}} = -2$ and C_{M}. The latter definitions allow us to write the ionic strength of the CS solutions in the following form:

$$I = \frac{1}{2}\left[2z_{\mathrm{H}}^2 C_{\mathrm{M}} + 2z_s^2 C_s\right], \qquad (38)$$

where $z_s = 1$ and C_s represent the charge and concentration of NaCl, respectively. Moreover, we can now define the screening parameter of the DLVO interactions between the monomers as

$$\kappa = \frac{1}{r_{\mathrm{D}}} = \sqrt{4\pi\lambda_{\mathrm{B}}(2z_{\mathrm{H}}^2 C_{\mathrm{M}} + 2z_s^2 C_s)}, \qquad (39)$$

where r_{D} is the Debye length. In Fig. 2 we show the GER0 results for the osmotic pressure in comparison to the osmotic pressure measurements of Chahine et al. [1] on aqueous CS-C solutions at a temperature of $T = 298$ K and at different concentrations of added salt. For the calculations, we employed the Eqs. (29)–(33) in conjunction with Eqs. (22) and (28), and chose the parameters $a = 5.5 \times 10^{-9}$ dm, $\lambda_{\mathrm{B}} = 7.02 \times 10^{-9}$ dm and $N = 32$, unless explicitly specified otherwise. To represent the experimental data, we used the following equation [1]:

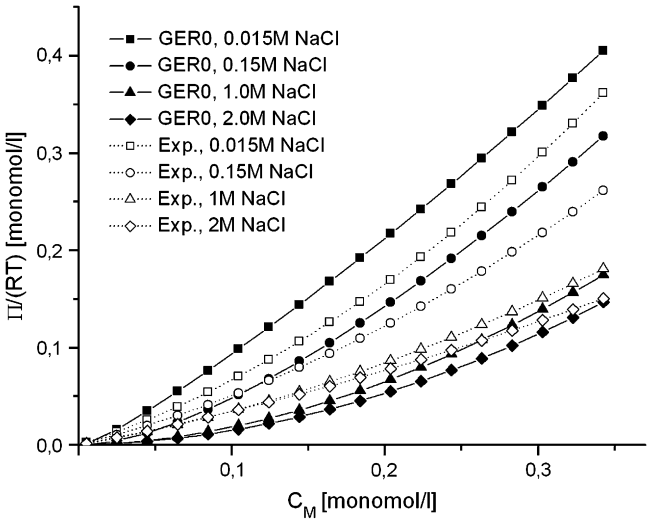

Fig. 2. Osmotic pressure as a function of monomer concentration at different salt concentrations, calculated with the GER0 method and compared to the experimental measurements of Chahine et al. [1].

$$\frac{\Pi}{RT} = \left[c_1|z_{\mathrm{M}}|C_{\mathrm{M}} + c_2 z_{\mathrm{M}}^2 C_{\mathrm{M}}^2\right]\frac{10^6}{RT}, \qquad (40)$$

where $|z_{\mathrm{M}}| = 2$. The coefficients c_1 and c_2 were taken from Table 1 in Ref. [1]. As we can deduce from the figure, the GER0 results agree qualitatively well with the experimental results of Chahine et al. [1] over the whole range of monomer and salt concentrations. This becomes particularly apparent, if we further compare in Fig. 3 the GER0 data with the molecular modeling data of Bathe et al. [5] as well as the experimental results of Chahine et al. in case of C4S solutions with the physiological salt concentration 0.15 M and 1 M. Bathe et al. performed their simulations at room temperature, using a canonical Metropolis Monte Carlo algorithm and employing periodic boundary conditions. For comparison, we used the molecular modeling results of Bathe et al. with chain lengths of $N = 16$ and $N = 32$ disaccharides, represented by the equation [5]

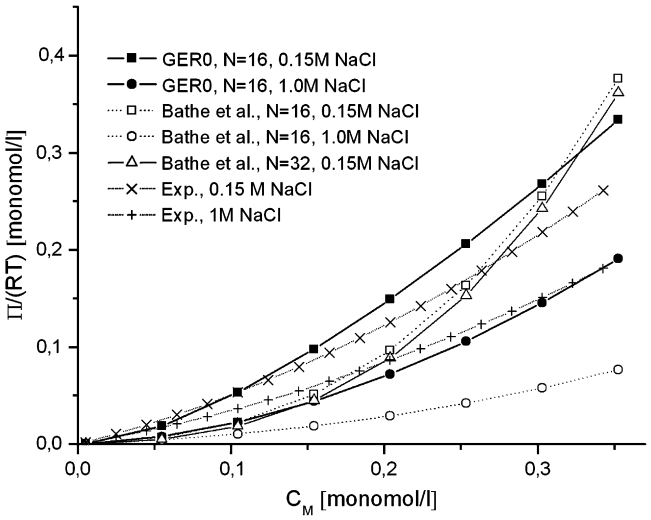

Fig. 3. Osmotic pressure as a function of monomer concentration at different salt concentrations, calculated with the GER0 method and compared to the experimental measurements of Chahine et al. [1], as well as the molecular modeling results of Bathe et al. [7].

$$\frac{\Pi}{RT} = A_1 c + A_2 c^2 + A_3 c^3, \tag{41}$$

where $c = C_M M$ is the polymer concentration with C_M as the monomolar concentration and $M = 457$ Da as the disaccharide molar mass. The coefficients A_1, A_2 and A_3 were taken from Tables 1 and 2 of Ref. [5]. We conclude from both graphs that the GER0 results are in better agreement with regard to experimental data, than the computer simulation results of Bathe et al. The reason of the failure of the molecular modeling method of Bathe et al. is in our view that it makes use of the mean field Poisson–Boltzmann (PB) theory, to evaluate the electrostatic interactions in the electrolyte medium surrounding the CS chains. This approach enhances the sampling of the conformational space of the CS chains by pre-averaging over the solvent degrees of freedom and eliminates the need to determine long-range Coulombic interactions through computationally expensive techniques, like the Ewald summation. Unfortunately, the underlying MF approximation not only increases the computational efficiency of their calculation procedure, but also neglects important *electrostatic correlation effects*, arising from density fluctuations of the counterions. Another consequence of the MF treatment is that the counterion condensation phenomenon cannot be taken into account appropriately in their molecular model, which leads to an underestimation of the contribution of the electrostatically induced stiffness to the osmotic pressure. Both shortcomings have been put forward by Bathe et al. as possible source of error of their calculation procedure [5,7]. In contrast to Bathe's approach, we take into account the electrostatic correlation effects between the counterion clouds of the CS chains by employing the method of GER, which treats our CS model beyond the MF level of approximation. As already mentioned in the Introduction, it relies on the concept of tadpole renormalization, which originates from quantum field theory, and is based on the observation that the main contributions to the partition function integral are provided by divergent low-order tadpole-type Feynman diagrams, arising from particle self-interactions. These divergences can effectively be taken into account by deriving the GER of the partition function integral, using the GER transformation procedure presented in Section 2.2. Its lowest order approximation, i.e. the GER0 approximation, has proven in several recent works to provide structural and thermodynamic information of higher accuracy than the MF approach at similar computational costs by including a tremendous amount of density correlation into the calculation [14,16,21,23]. We explain the remaining discrepancy between the GER0 and experimental data by the neglect of local electrostatic and solvent effects, inducing the solvent-mediated condensation of the counterions onto the CS chains and causing the dependence of the excluded volume parameter a on concentration. We will in the following take them into account in a coarse-grained fashion by introducing a concentration dependent *effective* excluded volume parameter a^{eff}. We interpret this latter parameter as the diameter of the cloud of counterions, condensed onto the CS chains that are subjected to local electrostatic and hydration effects. In Fig. 4 we show the osmotic pressure as a function of monomer concentration at different salt concentrations, obtained by adjusting the GER0 expressions in Eqs. (29)–(33) onto the experimental results through varying the effective excluded volume parameter introduced previously. We observe that the resulting *effective* GER0 approach describes the experimental data over the entire range of monomer concentrations and at all concentrations of added salt very well. In Fig. 5 we visualize the corresponding effective excluded volume parameter as a function of monomer concentration at various NaCl concentrations. We observe that at a salt concentration of 0.015 M the parameter goes to zero in the limit $C_M \to 0$, which can be explained by the fact that in this regime only

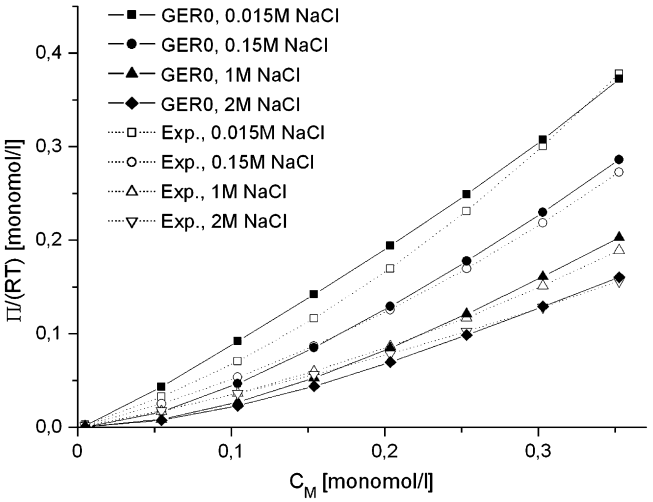

Fig. 4. Osmotic pressure as a function of monomer concentration at different salt concentrations, calculated with the effective GER0 method and compared to the experimental measurements of Chahine et al. [1].

the negatively charged CS chains with zero diameter contribute to the excluded volume. In this regime, the counterions are highly mobile and only loosely bound to the CS chains. This is due to the fact that in aqueous CS solutions at infinite dilution the ionic dissociation tendency, due to hydration, dominates over the counterion condensation phenomenon, which is in conformity with the Ostwald principle of dilution. Moreover, we further deduce from the graph that at this salt concentration the excluded volume parameter increases with growing monomer concentration C_M, due to condensation of the counterions onto the CS chains. By contrast, at higher concentrations of added salt we see that a^{eff} remains finite in the zero C_M limit. This relates to the high concentration of the counterions, causing that a part of them remains attached (condensed) onto the CS chains, down to vanishing monomer concentrations. We further deduce from the graph that at salt concentrations of 1 M and 2 M the excluded volume parameter decreases with increasing C_M. In this regime a large amount of condensed counterions has to share a decreasing amount of water molecules, which leads to a decrease in the

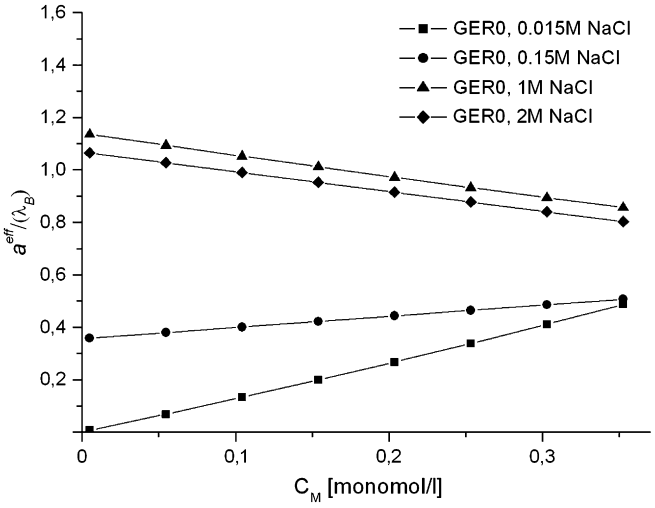

Fig. 5. Effective excluded volume parameter as a function of monomer concentration at different salt concentrations, determined with the effective GER0 method.

average size of their hydration shells. Finally, we recognize that at a salt concentration of approximately 0.15 M a turnover in behavior of the slope of the effective parameter a^{eff} takes place. It is worth pointing out that this salt concentration just coincides with the physiological salt concentration in the cartilage tissue [5]. In Fig. 6 we plot the dependence of the Debye length r_D, calculated via Eq. (39), on the monomer concentration at different salt concentrations. The quantity describes the distance of action of the electric field of each monomer charge within the electrolyte medium. Inside the sphere of radius equal to the Debye length, the hydrated counterions are directly exposed to the influence of the electric field of the CS monomers, while outside of it the electric field is shielded as a result of the polarization of the surrounding electrolyte medium. From the plot, we conclude that the Debye length increases with decreasing salt concentration. This is due to the evaporation tendency of the condensed counterions, caused by hydration. Moreover, we observe that the Debye length decreases with growing monomer concentration and that its rate of decrease diminishes with salt concentration. This relates to the fact that with higher salt concentration the availability of water molecules decreases, while the number of counterions increases. In Fig. 7 we show the molar excess entropy, calculated via Eq. (36), as a function of monomer concentration at the same NaCl concentrations as regarded previously. We recognize that at an added salt concentration of 0.015 M the entropy possesses three distinct regimes. After an initial phase of fast decrease, a plateau appears at a monomer concentration of $C_M \approx 0.05$ monomol/l, which is followed by another phase of accelerated decrease at $C_M > 0.3$ monomol/l. We attribute the three entropic regimes to the different structural arrangements of the CS chains, corresponding to the dilute, semidilute and concentrated regimes of polymer systems [25]. Finally, we observe that with increasing salt concentration the decrease of the entropy becomes slower and monotonic. This relates to the fact that at higher salt concentrations the monomer interactions are screened due to the counterions, causing that the distinct regimes of structural arrangement are suppressed.

Let us next analyze the consequences of our findings for the frictional–compressive properties of articular cartilage. We believe that in the optimal case CS in cartilage should have a low resistance against gliding and at the same time a high resistance against compression. We already noted from the curves of the Debye length that at 0.015 M the electrostatic friction is largest and, thus, the resistance against gliding would be largest in this case, which renders the moving of the joints more difficult. By contrast, at higher salt concentration the electrostatic friction becomes lower, but at the same time the osmotic pressure decreases, which leads to a decrease of the compressive resistance. In the following let us consider in Fig. 8(a) a sketch of the aggrecan layers as existing in the cartilage tissue on the macromolecular scale at the physiological salt concentration [26,27]. We assume that the condensed counterion cloud around each CS chain acts as an envelope, causing its *electrostatically induced stiffness*. Such an envelope should have in the ideal case a low gliding resistance, as well as a high resistance against compression. The former property allows a fast movement of opposing envelopes with low friction and minimal development of dissipative energy. The second property ensures that the CS molecules with their envelopes can absorb compressive shocks optimally, so that any risks of cartilage damaging are excluded. Both properties are optimized at the physiological salt concentration 0.15 M. At this concentration, the counterion evaporation is low and the diameter of the counterion clouds, expressed by the effective excluded volume parameter a^{eff}, remains nearly constant as the monomer concentration is increased. This relates to the fact that the CS chains during compression remain always nearly stretched due to the electrostatically induced stiffness, conferred by their condensed counterion clouds. In Fig. 8(b) and (c) we show sketches of the situation encountered in the cartilage tissue under low and high joint loading conditions, respectively. At low loads, the CS chains are fully stretched, to ensure optimal gliding and at the same time allow a high resistance against compression. At high loads, the CS chains react by squeezing out the water and reducing in this way their electrostatically induced stiffness, which causes that they become highly flexible and adopt a coil-like conformation in concordance with the natural functional role of CS in the cartilage tissue. It is worth noting in this context that the dominance of the electrostatic interactions in the mechanical stiffness of CS in the cartilage extracellular matrix has been confirmed in recent experimental works [11,27]. These ensure that the cartilage tissue can contract and act as a highly efficient shock absorber in the joints, conferring cartilage its characteristic mechanical properties. From the previous discussion, we can clearly conclude that, under the physiological conditions, the movement of the joints takes place at optimal frictional–compressive properties. A long-term deviation

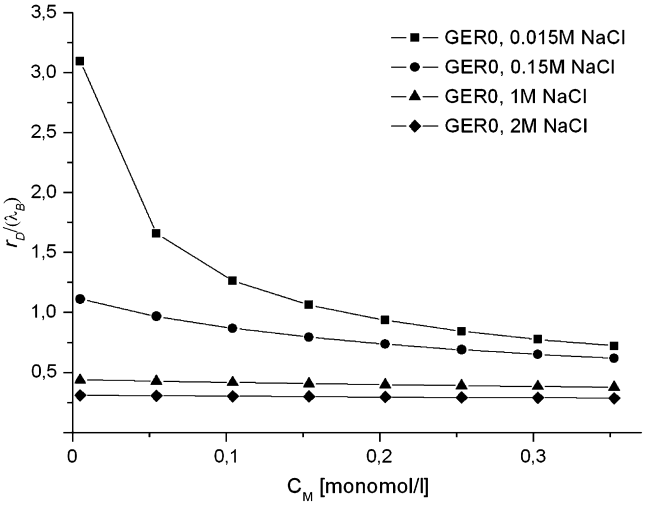

Fig. 6. Debye length, calculated with the GER0 method, as a function of monomer concentration at different salt concentrations.

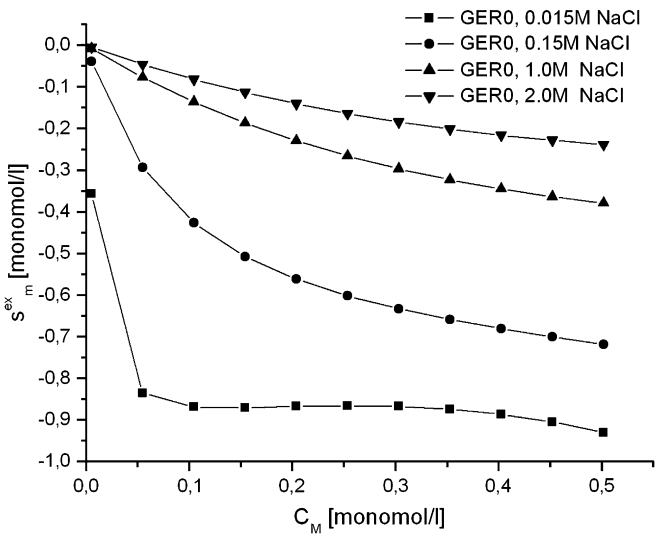

Fig. 7. Molar excess entropy, calculated with the GER0 method, as a function of monomer concentration at different salt concentrations.

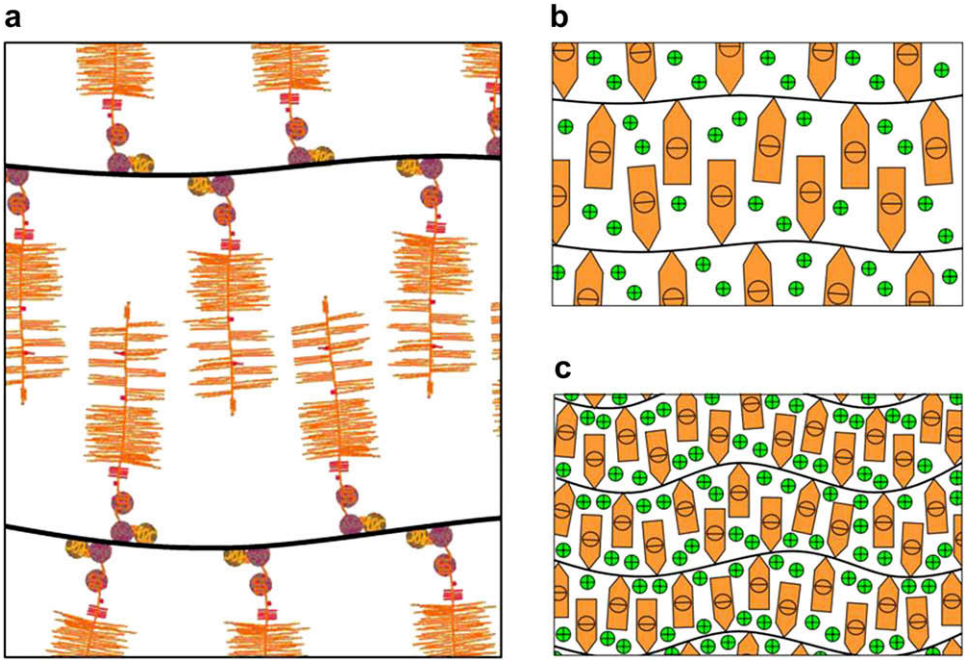

Fig. 8. Aggrecan layers in the cartilage tissue at the physiological salt concentration: (a) on the macromolecular scale, as well as subjected to (b) low and (c) high joint loadings. In the latter two figures green circles with plus signs denote counterions and orange arrows with minus signs the negatively charged aggrecan monomers (For interpretation of the references to colour in this figure legend, the reader is referred to the web version of this article).

from these conditions in the extracellular matrix, thus, may lead to a deterioration of the functionality of the CS molecules, which may trigger rheumatoid diseases. Ultimately, this could result in a loss of aggrecan, as often found in joint injuries or diseases, such as arthrosis, rheumatoid arthritis and osteoarthritis [28,29,30]. The apparent disfunction of the enzyme aggrecanase [30], which causes proteolytic cleavage of CS from aggrecan in the extracellular matrix leading to a high concentration of CS in the synovial fluid, could in our view also be the result of a regulation process of the enzyme in response to a change in the physiological or loading conditions. To increase the compressive performance of aggrecan in the cartilage tissue, the aggrecanase decreases the monomer concentration by cleaving CS from the aggrecan in the cartilage tissue. The cleaved aggrecan fragments are, then, transported into the synovial fluid. Unfortunately, at the same time the gliding resistance is augmented in the cartilage tissue, as a consequence of the increase of the electrostatic friction. This mechanism is supported by the research presented in this work.

4. Conclusions and outlook

In the present work we have studied the thermodynamic response of aqueous chondroitin sulfate solutions to changes in the monomer and added salt concentrations, using a recently developed field-theoretic approach beyond the mean field level of approximation. We have compared our calculation results to data from experiments as well as molecular dynamics calculations, and demonstrated that our method provides reliable information for the osmotic pressure and entropy. By adjusting the osmotic pressure to experimental data and analyzing the resulting effective excluded volume parameter in various concentration regimes, we have investigated the local electrostatic and solvent effects, influencing the condensation behavior of the counterions onto the chondroitin sulfate chains. This allowed us to draw important conclusions for the properties of these polyelectrolytes in aqueous solutions as well as in articular cartilage, which are summarized below.

First of all, we deduce from our investigation that the phenomenon of counterion condensation onto the chondroitin sulfate chains influences the thermodynamic as well as frictional–compressive properties of these systems in a crucial way. More specifically, we find that the counterion condensation behavior disappears in the limit of infinite dilution in solutions of low concentration of added salt, which is in opposition with the predictions of Manning's theory but in conformity with Ostwald's principle. Secondly, we find that with increasing salt concentration the counterions tend to condense onto the chondroitin sulfate chains, which decreases the electrostatic friction between the chains and, thus, their resistance against gliding. Moreover, we demonstrate that, at the same time, the hydration shells of the counterions become smaller, which diminishes the resistance of the chains against compression. Finally, we show that, at the physiological salt concentration, chondroitin sulfate solutions possess optimal frictional–compressive properties, which indicate that the phenomenon of counterion condensation onto the chondroitin sulfate chains has a major influence on the mechanical behavior of articular cartilage. These latter results provide support for the possibility that a long-term deviation from the physiological conditions in the cartilage tissue might trigger rheumatoid diseases.

Acknowledgments

We gratefully acknowledge the support of Prof. Dr. Buchner for offering helpful suggestions and encouragements.

References

[1] Chahine NO, Chen FH, Hung CT, Ateshian GA. Biophys J 2005;89:1543–50.
[2] Han L, Dean D, Mao P, Ortiz C, Grodzinsky AJ. Biophys J 2007;93:L23–5.
[3] Basalo IM, Chahine NO, Kaplun M, Chen FH, Hung CT, Ateshian GA. J Biomech 2007;40:1847–54.

[4] Hascall VC, Hascall GK. Proteoglycans. In: Hay ED, editor. Cell biology of extracellular matrix. New York: Plenum Press; 1981. p. 39–63.
[5] Bathe M, Rutledge GC, Grodzinsky AJ, Tidor B. Biophys J 2005;89:2357–71.
[6] Papagiannopoulos A, Waigh TA, Hardingham T, Heinrich M. Biomacromolecules 2006;7:2162–72.
[7] Bathe M, Rutledge GC, Grodzinsky AJ, Tidor B. Biophys J 2005;88:3870–87.
[8] Ehrlich S, Wolff N, Schneiderman R, Maroudas A, Parker KH, Winlove CP. Biorheology 1998;35:383–97.
[9] Donnan FG. Chem Rev 1924;1:73–90.
[10] Fixman M. J Chem Phys 1979;70:4995–5005.
[11] Jin M, Grodzinsky AJ. Macromolecules 2001;34:8330–9.
[12] Manning GS. J Chem Phys 1969;51:924–33.
[13] Stevens MJ, Kremer K. J Chem Phys 1995;103:1669–90.
[14] Baeurle SA, Nogovitsin EA. Polymer 2007;48:4883–99.
[15] Efimov GV, Nogovitsin EA. Physica A 1996;234:506–22.
[16] Baeurle SA, Efimov GV, Nogovitsin EA. Europhys Lett 2006;75:378–84.
[17] Baeurle SA, Kroener J. J Math Chem 2004;36:409–21.
[18] Dijkstra M, van Roij R. J Phys Condens Matter 1998;10:1219–28.
[19] Edwards SF. Proc Phys Soc London 1965;85:613–24.
[20] Baeurle SA. Int J Theor Phys 2002;41:1915–30.
[21] Baeurle SA, Charlot M, Nogovitsin EA. Phys Rev E 2007;75:011804.
[22] Baeurle SA. Phys Rev Lett 2002;89:080602.
[23] Baeurle SA, Efimov GV, Nogovitsin EA. J Chem Phys 2006;124:224110.
[24] Balescu R. Equilibrium and nonequilibrium statistical mechanics. New York: Wiley; 1975.
[25] Fredrickson GH. The equilibrium theory of inhomogeneous polymers. Oxford: Clarendon Press; 2006.
[26] Han L, Dean D, Daher LA, Grodzinsky AJ, Ortiz C. Biophys J 2008;95:4862–70.
[27] Seog J, Dean D, Rolauffs B, Wu T, Genzer J, Plaas AHK, et al. J Biomechanics 2005;38:1789–97.
[28] Saxne T, Heinegard D. Arthritis Rheum 1992;35:385–90.
[29] Saxne T, Glennas A, Kvien TK, Melby K, Heinegard D. Arthritis Rheum 1993;36:20–5.
[30] Lohmander LS, Neame PJ, Sandy JD. Arthritis Rheum 1993;36:1214–22.